Phase-diagram observation of liquid–liquid phase separation in the poly-L-lysine/ATP system and diagram-based application strategy

Tomohiro Nobeyama*[a], Tomohiro Furuki[a], and Kentaro Shiraki*[a]

T.N and T.F are first coauthors

[a] Dr.Tomohiro Nobeyama, Mr.Tomohiro Furuki and Prof.Dr.Kentaro Shiraki i
Faculty of Pure and Applied Sciences
University of Tsukuba
1-1-1 Tennodai, Tsukuba, Ibaraki 305-8573, Japan
E-mail: nobeyama.tomohiro.fu@u.tsukuba.ac.jp

Supporting information for this article is given via a link at the end of the document.

Abstract: Liquid–liquid phase separation (LLPS) is essential to understand biomacromolecule compartmentalization in living cells and to form soft-matter structures for chemical reactions and drug delivery systems. However, the importance of detail experimental phase diagrams of modern LLPS systems tend to be overlooked nowadays. Even for poly-L-lysine (PLL)/ATP system, one of the most widely used LLPS models, detailed phase diagram of LLPS have not been obtained. Herein, we report the first phase diagram of the (PLL)/ATP system and demonstrate the feasibility of phase-diagram based research design not only for understanding the physical properties of LLPS systems but also for realizing biophysical and medical applications. We established an experimental handy model of the droplet formation/disappearance process by forming a concentration gradient in a chamber as extracting a suitable condition on the phase-diagram including the two-phase droplet region. As a proof of concept of pharmaceutical application, we added a human immunoglobulin G (IgG) solution to PLL/ATP system. Using the knowledge of the phase diagram, we enabled to form IgG/PLL droplets clearly in the pharmaceutically required IgG concentration of ca. 10 mg/mL. This study provides a guidance for using the phase diagram to analyze and utilize LLPS

Liquid–liquid phase separation (LLPS) of biomacromolecules[1-5] such as DNA, RNA, and proteins plays key roles in sophisticated biological processes in real cells, including transcription,[6] compartmentalization of multiple enzymes, stress response,[7] and enzymatic reactions.[8,9] LLPS induces the formation of three-dimensional sphere-shaped dense structures dispersed in dilute phase,[1,10] which are called LLPS droplets or simply droplets. The peculiar physical states of LLPS droplets are responsible for processes such as reactant accumulation, compartmentalization of several enzymes, activation and deactivation of enzymatic activities,[8] and maturation of proteins into gels or fibrils.[3] Therefore, developing experimental models of biomacromolecule LLPS droplets to perform biophysical analysis in vitro have been desired.

The poly-L-lysine/adenosine-5-phosphate (PLL/ATP) system is a widely used in vitro model of LLPS. Mixing PLL and ATP solutions in an adequate ratio and concentration causes phase separation,[11] enabling the constitution of membrane-less organelles,[12,13] coacervate organelles in liposomes,[14,15] the design of sequential enzymatic reactions in droplets,[15] and the investigation of droplet formation/disappearance related to enzymatic reactions[16,17] and pH sensitivity of droplets in model cell membranes.[18] Although the experimental conditions for droplet formation have been investigated,[11,13,15], the LLPS phase diagram for the PLL/ATP system has surprisingly not been reported to date. Especially, high-concentration conditions like in cytosol or nuclei have not been studied, despite the relevance of the LLPS behavior in high-concentration regions such as reentrant LLPS regions.[19] Moreover, the PLL/ATP system is a good model of phase separation of proteins and nucleic acids in living cells.

Herein, we report the first LLPS phase diagram of the PLL/ATP system from low to high concentrations. The previously overlooked information on the physical behavior of LLPS systems provides new insights into the design of chemical systems related to LLSP droplets and the role of LLPS droplet formation in the biophysics and chemical biology fields. We performed microscopic assays in a silicon sheet chamber on a slide glass to observe the LLPS behavior in detail. We also examined the NaCl resistance of LLPS droplets in the PLL/ATP system, where droplets formed by oppositely charged biomolecules usually dissolve under high salt concentration. By reconstructing component gradient as across the two-phase droplet region on phase diagram in a chamber, we built a model of the nonequilibrium droplet formation/disappearance process based on direct microscopy observation. The phase diagram is also important in the preparation of antibody-containing coacervates for constructing antibody drug delivery systems (DDSs).[20]

First, we constructed a phase diagram of the PLL/ATP system by changing the concentration of PLL and ATP (Figure 1) from 0 to 100 mg/mL and from 0 to 1 M, respectively, as shown in Figure 1A. The value of vertical and horizontal lines was a final concentration of a 1:1 mixture of these two

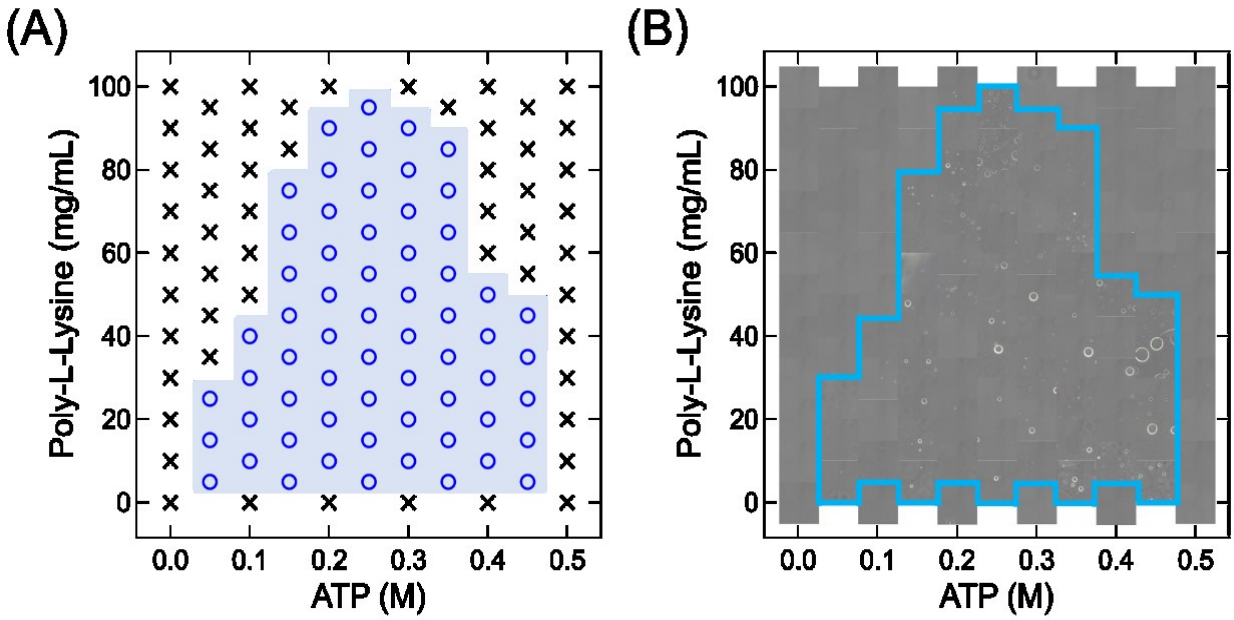

Figure 1. (A) Phase diagram of the PLL/ATP system. Circle points indicate the formation of droplets and cross points indicate the absence of droplets. Phase-separated region is shown in blue. (B) Pictures of the PLL/ATP mixture under the conditions of the phase diagram.

solutions. The phase diagram clearly shows the boundary of the visible LLPS droplet formation area. Figure 1B shows photographs recorded under the conditions of each point of the phase diagram.

PLL/ATP droplet formation is associated with the charge correlation between cationic protonated lysine and anionic deprotonated phosphoric acid of ATP. PLL/ATP droplets dissolve by adding ions such as NaCl; hence, it is worthwhile to investigate the phase diagram of PLL/ATP system with ions. We studied the formation of droplets in the presence of NaCl using ATP solutions containing NaCl at concentrations of 31.3, 100, 187.5, 250, and 500 mM, which were mixed with PLL solution in a 1:1 ratio to construct the phase diagrams shown in Figure 2. The boundary region of the droplet formation phase turned to a non-droplet phase even with only 31.3 mM NaCl, and the droplet phase region decreased as the NaCl concentration increased until showing no droplet formation at a NaCl concentration of 500 mM. These results are the first evidence for the dependence of the salt resistance of droplets on the salt concentration, indicating that the boundary area and the bottom area of the original phase diagram showed the weakest and the strongest resistance, respectively.

Generally, researchers have focused on the difference between droplet and non-droplet phases but have overlooked

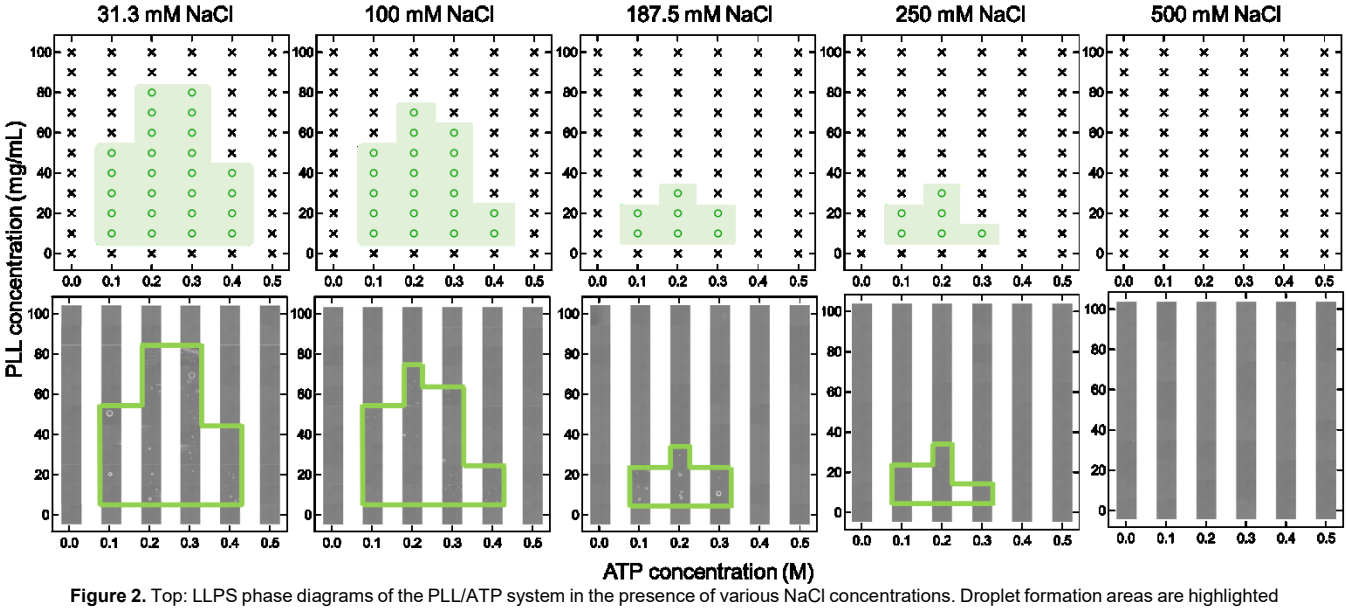

Figure 2. Top: LLPS phase diagrams of the PLL/ATP system in the presence of various NaCl concentrations. Droplet formation areas are highlighted in green. Bottom: pictures of the PLL/ATP system under the conditions of each phase diagram. Droplets are enclosed by the green lines.

the difference in the droplet characteristics depending on the

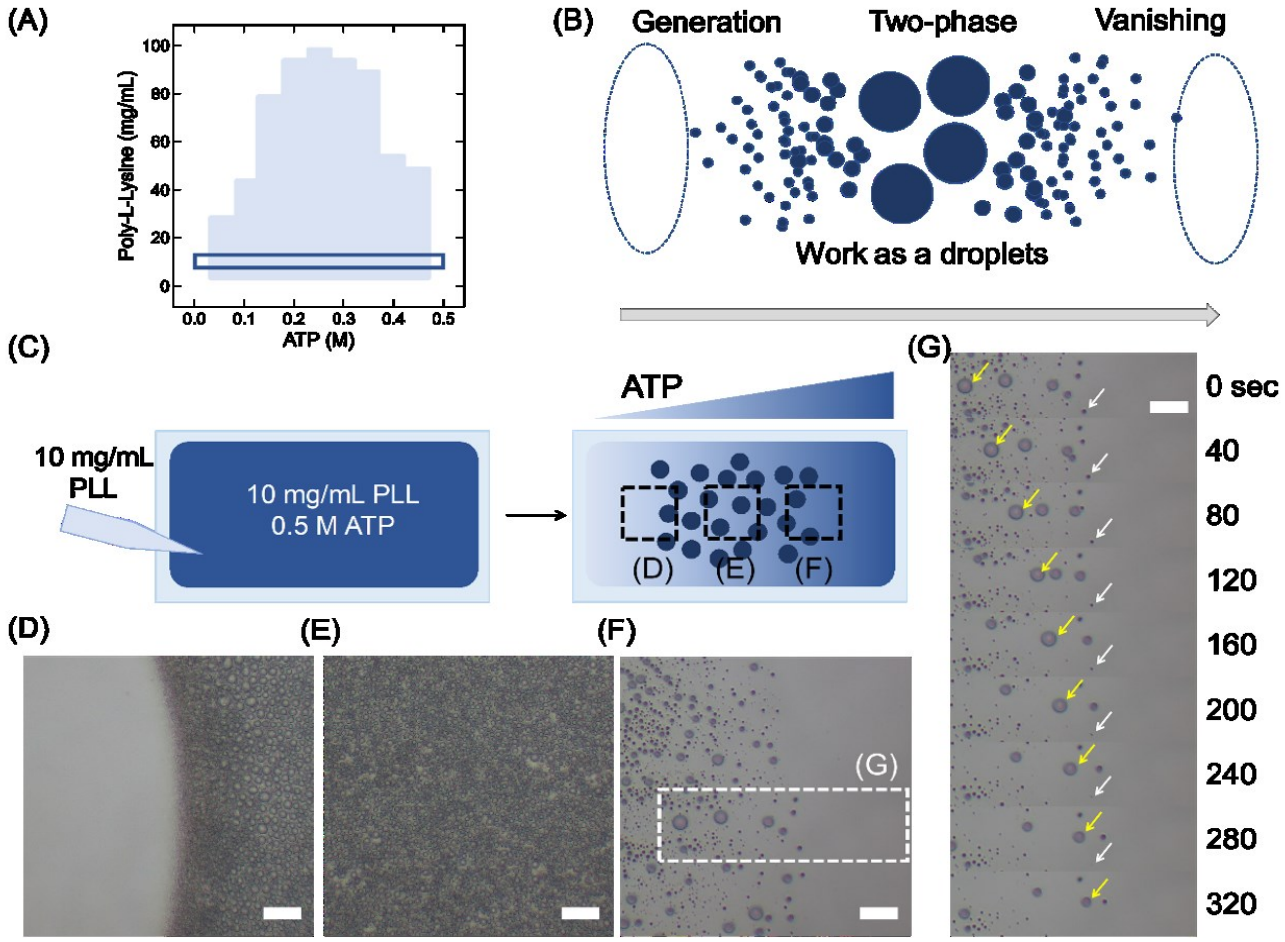

Figure 3. Phase-diagram-based modeling of nonequilibrium formation/disappearance process of droplets. (A) Phase diagram of PLL/ATP system and focused area enclosed by the line. (B) Schematic image of droplet life in real cells. Droplets are generated in a nonequilibrium process and are stable for a while until disappearing. (C) Experimental system of the observation of droplet formation, stable phase separation, and disappearance in one chamber according with the ATP and PLL concentration gradients. (D) Droplet formation with increasing ATP-to-PLL ratio. The boundary of droplet area and one-phase solution area corresponds to the boundary of the two-phase region of the PLL/ATP phase diagram. Many small droplets are generated at around boundary region. The droplets moves to the side of high concentration of ATP. (E) Stable phase separation area containing many stable droplets that appear motionless. (F) Droplet disappearance with the ATP and PLL concentration gradients. The boundary of the droplet and non-droplet areas corresponds to the domain boundary of the two-phase region of the PLL/ATP diagram. (G) Time course of droplet formation. Large droplets (yellow arrows) move to the side of high concentration of ATP.

component ratio. Our results suggest that the characteristics of the droplets formed via LLPS vary with the conditions. This data showed that droplets formed in a cell have various characteristics depending on the local concentration of macromolecules and droplets even from the same components could behave various way to outward stimulus like stress and/or accumulation of metabolites Careful obtaining of phase diagram of LLPS would provide such information

Next, according to the phase diagram, we established an experimental system to observe the nonequilibrium process of droplet formation and disappearance, which occurs in real cells (Figure 3, S1, Supplemental movies 1 and 2). We used an ATP and PLL concentration gradient in a chamber to mimic all phase boundaries and inner and outer areas of the two-phase diagram shown in Figure 3A to model the nonequilibrium process of the droplet life (Figure 3B).

In a real cell, droplets are generally generated under stimuli such as protein expression, accumulation, RNA translation, and epigenetic DNA modification and serve as reaction fields and for material storage.[6,21,22] Then, their disappearance is triggered by unknown reasons (Figure 3B), although local temperature changes or accumulation of metabolic products have been proposed as responsible.[15,23-25]

The droplet formation/disappearance process is essentially a nonequilibrium process. Some theoretical studies and molecular dynamics simulations have addressed this dynamic process; [26-28] however, experimental models to reproduce the droplet formation/disappearance process in vitro are scarce.

Using the phase diagram of the PLL/ATP system, we established a model system to reproduce the droplet formation/disappearance in a chip (Figure 3A and 3C). We filled a small chamber with a PLL/ATP solution mixture containing no droplet and then added an ATP solution gently from one side of the chamber. Concentration gradients and a boundary between the one-phase and two-phase regions

formed naturally. Observation of the boundary helps predict the droplet formation/disappearance in the chamber.

On the boundary at the lower ATP concentration side, small droplets were generated from the boundary and continuously larger on the right side (Figure 3D, supplemental movie 1). As the two solutions mixed, the boundary itself also moved gradually toward the PLL injected side (supplemental movie 2). Large droplets fell on the bottom slide glass of the chamber and expanded there. At the center of the chamber, droplets were stable (Figure 3E).

In contrast, the disappearance of droplets was observed near the opposite side boundary (Figure 3F). Large droplets moved toward the ATP-rich area and then disappeared (Supplemental movie 2). Larger droplets moved faster (Figure 3G), indicating that the velocity of droplet movement depends on the droplet radius (Figure S1A). Although the reason for the droplet motion remains unclear, this observation suggests that the motion of larger droplets stems from Marangoni convections on the droplet surface, while smaller droplets flow with the diffusion of ATP from the less viscous ATP solution to the PLL-rich direction. Our analysis suggests that the speed correlates with the droplet radius (Figure S1B) and it supported the occurrence of Marangoni convection in our system.[29] Note that some very small droplets moved in the opposite direction, against the ATP concentration gradient. Thus, we concluded that the smalls flowed with the usual diffusion of ATP toward low-concentration regions (Supplementary movie 2).

This observation-based phase-diagram modeling constitutes the profitable strategy to construct experimental handy model of the nonequilibrium process of droplet formation/disappearance, which could be applied to outward materials such as proteins, nanomaterials, and their complexes for the analysis of their interference on the LLPS process in real cells.

Droplets have gathered attention as a new category of DDSs.[20,30] In particular, the incorporation of immunoglobulin G (IgG), which is widely used as a component of antibody drugs, is an emerging demand.[31,32] Recently, LLPS-induced IgG-FcB(L17E) condensates were proposed as a new DDS carrier of antibody drugs to increase cytosolic delivery activity.[20] To evaluate the applicability of our phase-diagram-based droplet design in medicine, we prepared IgG droplets by adding an IgG solution to the PLL/ATP mixture and monitored the formation of IgG droplets, dispersions, or aggregates (Figure 4, Figure S2). After mixing ATP and PLL solutions, we added and mixed a 1/10 volume of a 100 mg/mL IgG solution containing ca. 1% of rhodamine-labeled fluorescent IgG for observation.

Going straight to the point, upper one-phase region was suitable area to incorporate IgG to PLL/ATP system droplets. Surprisingly, no incorporation of IgG into PLL/ATP droplets was observed in the original two-phase region, whereas in the PLL richer area, which originally showed no phase separation, IgG droplets were formed (Figure 4A). PLL was located according to its autofluorescence, which results from the inter- and intra-hydrogen bonding network of PLL molecules.[33,34] IgG molecules dispersed or aggregated in almost all of original two phase (Figure S2). As an exception, at an ATP final concentration of 0.14 M, IgG molecules were gathered on the droplet surface, causing PLL/ATP droplet aggregation (Figure 4B and S2).

In the PLL-rich area, the upper region in the original two-phase area, IgG formed clear droplets with PLL (Figure 4C). Interestingly, the droplets formed a double layer at low ATP concentrations (e.g., in 0.04 mM ATP solution) but a single

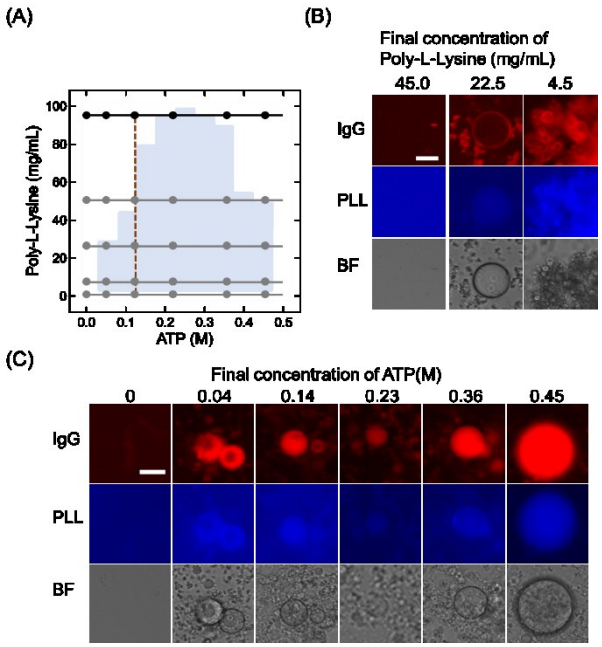

Figure 4. IgG incorporation in PLL/ATP droplets. (A) Phase diagram of PLL/ATP system after addition of 10 mg/mL IgG. The blue area indicates the phase separation area of the original PLL/ATP system. The black and gray dots are observed points. The brown dotted line in the phase diagram corresponds to panel B, and the black straight line corresponds to panel C. (B) IgG accumulation on the surface of PLL/ATP droplets in the inner part of the original phase separated area. PLL was monitored by its autofluorescence. BF indicates bright-field microscope images. (C) IgG droplet generation in the upper region from the original phase-separated area. PLL final concentration was 95 mg/mL. IgG and PLL were colocalized in single- and double-layer droplets generated upon adding IgG at PLL 95 mg/mL condition.

layer at high ATP solutions. PLL was located in IgG-rich areas in both single- and double-layer droplets.

These data indicate that phase diagrams can be used to design droplet-based systems. In this example of IgG embracing, we had to utilize the originally one-phase condition. By contrast, the two-phase condition in the phase diagram only formed the aggregation of IgG (Figure S3). They indicated that a previous grasp of a phase diagram and focused on one phase region upper the phase diagram is profitable to generate droplets with additional proteins. This is a good example to tell us the significance of depicting the phase diagram carefully before applying an LLPS system to advanced applications. LLPS droplets are related not only to biophysics[35] but also to synthetic biology and chemical biology for material production,[16] analysis of droplet-enzyme formation,[8,15,36] and medicinal applications.[20,37] Gaining insight into the formation/disappearance and behavior of droplets is essential for the rational design of systems related to LLPS droplets. Other few examples of experimental phase diagram observation for the study of LLPS also have shown informative insights.[19,38-40] In this study, we developed a phase-diagram-based approach to understand and predict

LLPS systems for biophysical and biochemical applications. Using a classical PLL/ATP system, we constructed a LLPS phase diagram and investigated the concentration dependency of the salt resistance of PLL/ATP droplets for the first time. Then, we applied the phase diagram to the development of a model to predict the droplet formation/disappearance dynamics, which has potential application in the fields of biology and physics. We also revealed that the antibody incorporation into droplets can be predicted according to the phase diagram. For instance, the conditions of the upper area of the two-phase region in the phase diagram of the PLL/ATP system were suitable for IgG incorporation.

Acknowledgements

We are grateful for the kind support of Toyama Prefectural University, Kyoto University, and the University of Tsukuba. We are grateful for the academic and supportive atmosphere afforded by Kumano Dormitory at Kyoto University. This study was supported by the KAKENHI of the Japan Society for the Promotion of Science (JSPS) to T.N. (21J00852) and K. S. (22K19284)

We would like to thank Enago (www.enago.jp) for the English language review.

Keywords: liquid–liquid • phase separation • poly-L-lysine/ATP system• phase diagrams • nonequilibrium processes • drug delivery

References

[1] Y. Shin, C. P. Brangwynne, *Science* **2017**, *357*.
[2] A. A. Hyman, C. A. Weber, F. Jülicher, *Annu. Rev. Cell Dev. Biol.* 2014, *30*, pp 39–58.
[3] W. M. Babinchak, W. K. Surewicz, *J. Mol. Biol.* **2020**, *432*, pp 1910–1925.
[4] C. D. Crowe, C. D. Keating, **2018**, *8*, p 20180032.
[5] Y. R. Kamimura, M. Kanai, *Bull. Chem. Soc. Jpn.* **2021**, *94*, pp 1045–1058.
[6] J. Berry, S. C. Weber, N. Vaidya, M. Haataja, C. P. Brangwynne, *Proc. Natl. Acad. Sci. U. S. A.* **2015**, *112*, pp E5237–E5245.
[7] J. R. Wheeler, T. Matheny, S. Jain, R. Abrisch, R. Parker, *eLife* **2016**, *5*.
[8] A. M. Küffner, M. Prodan, R. Zuccarini, U. Capasso Palmiero, L. Faltova, P. Arosio, *ChemSystemsChem* **2020**, *2*.
[9] A. Testa, M. Dindo, A. A. Rebane, B. Nasouri, R. W. Style, R. Golestanian, E. R. Dufresne, P. Laurino, *Nat. Commun.* **2021**, *12*, p 6293.
[10] C. P. Brangwynne, P. Tompa, R. V. Pappu, *Nat. Phys.* **2015**, *11*, pp 899–904.
[11] S. Koga, D. S. Williams, A. W. Perriman, S. Mann, *Nat. Chem.* **2011**, *3*, pp 720–724.
[12] T. Lu, K. K. Nakashima, E. Spruijt, *J. Phys. Chem. B* **2021**, *125*, pp 3080–3091.
[13] R. S. Fisher, S. Elbaum-Garfinkle, *Nat. Commun.* **2020**, *11*, p 4628.
[14] N. N. Deng, W. T. S. Huck, *Angew. Chem. Int. Ed. Engl.* **2017**, *56*, pp 9736–9740.
[15] T. Ura, S. Tomita, K. Shiraki, *Chem. Commun. (Camb.)* **2021**, *57*, pp 12544–12547.
[16] H. Karoui, M. J. Seck, N. Martin, *Chem. Sci.* **2021**, *12*, pp 2794–2802.
[17] K. K. Nakashima, J. F. Baaij, E. Spruijt, *Soft Matter* **2018**, *14*, pp 361–367.
[18] M. G. F. Last, S. Deshpande, C. Dekker, *ACS Nano* **2020**, *14*, pp 4487–4498.
[19] G. Krainer, T. J. Welsh, J. A. Joseph, J. R. Espinosa, S. Wittmann, E. de Csilléry, A. Sridhar, Z. Toprakcioglu, G. Gudiškytė, M. A. Czekalska, W. E. Arter, J. Guillén-Boixet, T. M. Franzmann, S. Qamar, P. S. George-Hyslop, A. A. Hyman, R. Collepardo-Guevara, S. Alberti, T. P. J. Knowles, *Nat. Commun.* **2021**, *12*, p 1085.
[20] T. Iwata, H. Hirose, K. Sakamoto, Y. Hirai, J. V. V. Arafiles, M. Akishiba, M. Imanishi, S. Futaki, *Angew. Chem. Int. Ed. Engl.* **2021**, *60*, pp 19804–19812.
[21] X. Li, Z. An, W. Zhang, F. Li, *Genes (Basel)* **2023**, *14*.
[22] E. Gomes, J. Shorter, *J. Biol. Chem.* **2019**, *294*, pp 7115–7127.
[23] Y. Shen, F. S. Ruggeri, D. Vigolo, A. Kamada, S. Qamar, A. Levin, C. Iserman, S. Alberti, P. S. George-Hyslop, T. P. J. Knowles, *Nat. Nanotechnol.* **2020**, *15*, pp 841–847.
[24] W. K. Spoelstra, E. O. van der Sluis, M. Dogterom, L. Reese, *Langmuir* **2020**, *36*, pp 1956–1964.
[25] S. Cinar, H. Cinar, H. S. Chan, R. Winter, *J. Am. Chem. Soc.* **2019**, *141*, pp 7347–7354.
[26] M. Farshad, M. J. DelloStritto, A. Suma, V. Carnevale, *J. Phys. Chem. B* **2023,** *127*, pp 3682–3689.
[27] Q. Guo, G. Zou, X. Qian, S. Chen, H. Gao, J. Yu, *Nat. Commun.* **2022**, *13*, p 5771.
[28] T. J. Welsh, G. Krainer, J. R. Espinosa, J. A. Joseph, A. Sridhar, M. Jahnel, W. E. Arter, K. L. Saar, S. Alberti, R. Collepardo-Guevara, T. P. J. Knowles, *Nano Lett.* **2022,** *22*, pp 612–621.
[29] A. May, J. Hartmann, S. Hardt, *Soft Matter* **2022**, *18*, pp 6313–6317.
[30] Y. Sun, S. Y. Lau, Z. W. Lim, S. C. Chang, F. Ghadessy, A. Partridge, A. Miserez, *Nat. Chem.* **2022**, *14*, pp 274–283.
[31] A. Beck, L. Goetsch, C. Dumontet, N. Corvaïa, *Nat. Rev. Drug Discov.* **2017**, *16*, pp 315–337.
[32] W. Wang, E. Q. Wang, J. P. Balthasar, *Clin. Pharmacol. Ther.* **2008**, *84*, pp 548–558.
[33] U. N. Morzan, G. Díaz Mirón, L. Grisanti, M. C. González Lebrero, G. S. Kaminski Schierle, A. Hassanali, *J. Phys. Chem. B* **2022**, *126*, pp 7203–7211.
[34] L. Homchaudhuri, R. Swaminathan, *Chem. Lett.* **2001**, *30*, pp 844–845.
[35] G. L. Dignon, R. B. Best, J. Mittal, *Annu. Rev. Phys. Chem.* **2020**, *71*, pp 53–75.
[36] K. K. Nakashima, M. A. Vibhute, E. Spruijt, *Front. Mol. Biosci.* **2019**, *6*, p 21.
[37] S. Alberti, D. Dormann, *Annu. Rev. Genet.* **2019**, *53*, pp 171–194.
[38] H. Cinar, R. Winter, *Sci. Rep.* **2020**, *10*, p 17245.
[39] H. Zhang, F. Wang, B. Nestler, *Langmuir* **2022**, *38*, pp 6882–6895.
[40] S. Mondal, K. Narayan, S. Botterbusch, I. Powers, J. Zheng, H. P. James, R. Jin, T. Baumgart, *Nat. Commun.* **2022**, *13*, p 5017.

Entry for the Table of Contents